Structure of carbohydrate-bound polynuclear iron oxyhydroxide nanoparticles in parenteral formulations

Dina S. Kudasheva [a,b], Jriuan Lai [a,b,c], Abraham Ulman [a,b,c], Mary K. Cowman [a,b,*]

[a] Othmer Department of Chemical and Biological Sciences and Engineering, Polytechnic University, Six Metrotech Center, Brooklyn, NY 11201, USA
[b] Herman F. Mark Polymer Research Institute, Polytechnic University, Six Metrotech Center, Brooklyn, NY 11201, USA
[c] The NSF MRSEC for Polymers at Engineered Interfaces, Polytechnic University, Six Metrotech Center, Brooklyn, NY 11201, USA

Abstract

Intravenous iron therapy is used to treat anemia associated with chronic kidney disease. The chemical structures of parenteral iron agents have not been characterized in detail, and correlations between structure, efficiency of iron delivery, and toxicity via catalysis of oxygen-derived free radical creation remain to be established. In this study, two formulations of parenteral iron have been characterized by absorption spectroscopy, X-ray diffraction analysis (XRD), transmission electron microscopy (TEM), atomic force microscopy (AFM), and elemental analysis. The samples studied were Venofer® (Iron Sucrose Injection, USP) and Ferrlecit® (Sodium Ferric Gluconate in Sucrose Injection). The 250–800-nm absorption spectra and the XRD patterns showed that both formulations contain a mineral core composed of iron oxyhydroxide in the β-FeOOH mineral polymorph known as akaganeite. This was further confirmed for each formulation by imaging using TEM and AFM. The average core size for the nanoparticles, after dialysis to remove unbound or loosely bound carbohydrate, was approximately 3 ± 2 nm for the iron–sucrose, and approximately 2 ± 1 nm for the iron–gluconate. Each of the nanoparticles consists of a mineral core, surrounded by a layer of bound carbohydrate. The overall diameter of the average bead in the dialyzed preparations was approximately 7 ± 4 nm for the iron–sucrose, and 3 ± 1 nm for the iron–gluconate. Undialyzed preparations have particles with larger average sizes, depending on the extent of dilution of unbound and loosely bound carbohydrate. At a dilution corresponding to a final Fe concentration of 5 mg/mL, the average particle diameter in the iron–sucrose formulation was approximately 22 ± 9 nm, whereas that of the iron–gluconate formulation was approximately 12 ± 5 nm.
© 2004 Elsevier Inc. All rights reserved.

Keywords: Parenteral formulations; Iron oxyhydroxide; Iron–carbohydrate complex; AFM; Iron–sucrose injection; Sodium ferric gluconate; Akaganeite

1. Introduction

Parenteral iron formulations containing iron complexed to monosaccharides or disaccharides are among the products currently used for the treatment of anemia.

Yet, the chemical structures of these materials have not been characterized in detail, and correlations between structure and complex stability, efficiency of iron delivery, and toxicity via catalysis of oxygen-derived free radical creation remain to be established. This study represents a first step toward complete characterization of the structures of this subclass of modern therapeutic iron–carbohydrate compounds.

Iron(III) oxyhydroxide is formed in aqueous solutions by the dissolution of a suitable iron salt, such as ferric chloride, at low pH, followed by neutralization

2. Materials and methods

The parenteral iron formulations used in this study were an iron–sucrose (Venofer®, Iron Sucrose Injection, USP, lots 1644 and 2323A), from American Regent, Inc., Shirley, NY, and an iron–gluconate in sucrose (Ferrlecit®, Sodium Ferric Gluconate Complex in Sucrose Injection, lots 1F541 and 1C239), from Watson Pharmaceuticals, Inc., Corona, CA. Venofer® was supplied as the iron–sucrose complex in 5 mL vials containing 100 mg of elemental iron in 30% sucrose solution (20 mg Fe/mL) at a pH of about 10.5–11.1. The apparent average molecular mass is stated in the package insert to be 34–60 kDa. Ferrlecit® was obtained as the iron–gluconate complex in 5 mL ampules containing 62.5 mg of elemental iron as a sodium salt of a ferric gluconate complex in 20% sucrose (12.5 mg Fe/mL) at a pH of about 7.7–9.7. The apparent average molecular mass is stated in the package insert to be 350 ± 23 kDa. Some samples, where noted in the text, were subjected to dialysis to remove low molecular mass components. Dialysis of samples for absorption spectroscopy was performed against deionized water, at a pH of about 5.4, in Slide-A-Lyzer Dialysis Cassettes (Pierce, Rockford, IL) made of low-binding regenerated cellulose membrane, molecular weight cutoff (MWCO) 10,000. Cassette capacity was 0.5–3 mL. Larger volumes of dialyzed samples were needed for AFM and TEM studies; in that case dialysis against deionized water at neutral pH, or with pH adjusted with KOH to match the sample pH, was performed in tubes made of Spectra/Por Molecularporous Regenerated Cellulose Membrane (Spectrum Laboratories Inc., Rancho Domingues, CA) with MWCO 6–8,000. Dialysis time for both trials was 20–48 h. Dialyzed samples were sent to Huffman Laboratories, Inc. (Golden, CO) for elemental analysis to determine the amount of iron, carbon and sodium.

Absorption spectra were recorded on a Perkin–Elmer Lambda 800 UV/VIS absorption spectrophotometer. The spectra were analyzed with UV WinLab software v3.00.03. The spectra were recorded in the range of 800–200 nm for original non-diluted samples and for diluted or dialyzed samples. This instrument has the ability to analyze samples with relatively high absorbance. Its photometric linearity at an absorbance (A) of 3 is ± 0.006 A units and at A of 2 is ± 0.002 A units. The photometric accuracy at A of 2 is ± 0.003 A units and stray light in the range of 220–370 nm is <0.00008% T. The photometric range is ± 7 A. For the undiluted samples, cylindrical quartz cells of path length 0.001 or 0.01 cm were employed; for all other samples a cylindrical quartz cell of path length 0.01 cm was used. The reference was water. All spectra were recorded as absorbance vs. wavelength of light in nm. Molar extinction coefficients were calculated from the absorbances at wavelengths of 300 and 470 nm, based on the molar concentration of iron in each sample. The molar iron concentrations were calculated from the stated weight concentration of iron in each sample.

X-ray powder diffraction (XRD) patterns were recorded at a scanning rate of $0.008°\,min^{-1}$ in the range 2θ from $0°$ to $70°$ using a Philips X-ray diffractometer with Cu Kα radiation ($\lambda = 1.5418$ Å). Original and dialyzed samples were prepared by freeze-drying prior to analysis. The average iron mineral crystallite size, D, was calculated from the observed XRD profiles using the peak full width at half maximum height (β) of the selected diffraction peak, using the Scherrer formula [23]:

$$D = K\lambda/\beta\cos\theta,$$

where K is the Scherrer constant, with a value of 0.94. For recorded crystalline patterns, diffraction angles and interplanar spacings obtained were compared with the values compiled in the JCPDS-ICDD (Joint Committee on Powder Diffraction Standard-International Center for Diffraction Data-copyright PSI International) reference cards.

Electron microscopic studies of the iron-core crystal size and morphology for the iron–carbohydrate samples were carried out by using a Phillips CM-12 Transmission Electron Microscope (100 keV). All preparations were deposited one night before imaging onto a carbon stabilized Formvar-coated copper grid (400 mesh), purchased from Ted Pella, Inc., Redding, CA. Approximate grid hole size is 42 μm, and the thickness of Formvar films stabilized with carbon is 5–10 nm. All attempts to image the original undiluted liquids were not successful, because the resulting film on a grid was too thick for electrons to penetrate. Consequently, the iron–carbohydrate complexes were dialyzed and the grid was dipped into the sample and then the excess liquid was removed with a very gentle flow of compressed nitrogen.

Atomic force microscopy (AFM) was used to determine size and shape of iron–carbohydrate complexes. The instrument used was a MultiMode Scanning Probe Microscope with Nanoscope IIIa controller and a type EV scanner (Veeco Instruments, Inc). The scanner was calibrated in the x–y plane using the 1 μm etched grid, and in the z-direction using the 200 nm height calibration standard. The samples for imaging were prepared in two ways. In the first procedure, samples were diluted 2 to 80-fold with deionized water prior to analysis. In the second procedure, samples were dialyzed against deionized water prior to analysis. In both cases, 4 μL of sample was put on a freshly cleaved mica surface, then after 20–30 s the surface was rinsed with 100 μL of deionized water to get rid of unbound particles, and the surface was dried by a gentle flow of nitrogen. The AFM imaging technique used was Tapping Mode™. TESP etched silicon cantilever probes of 125 μm nominal length were used, at a drive frequency of approximately 240–280 kHz. We generally use an RMS (root

Table 1
Characterization of iron–carbohydrate complexes by absorption spectroscopy

Sample	Fe Conc. (mg/mL)	Cell path length (cm)	ε_{300} (M^{-1} cm^{-1})	ε_{470} (M^{-1} cm^{-1})	$\varepsilon_{300}/\varepsilon_{470}$
Iron–sucrose	20	0.001	2990		7.9
	20	0.01		380	
	5	0.01	2720	390	7.0
Iron–gluconate	12.5	0.001	2600		9.0
	12.5	0.01		290	
	5	0.01	2670	250	10.6

charge transfer absorption band. There is no evidence for the existence of low spin state Fe(III) or for aquated Fe(II). The shapes of the spectra are essentially the same for both iron–carbohydrate samples; both formulations showed characteristic absorption spectra expected for Fe(III) complexes in an octahedral d^5 high spin state.

The position of the d–d transition band around 500 nm has been shown to depend on the distance between two neighboring Fe atoms [26]. Thus, in the case of face-sharing octahedra of an iron oxide hematite, this band is above 500 nm. For the edge- and corner-sharing octahedra and hence larger Fe–Fe distances in iron oxyhydroxides this transition is weaker and lies at shorter wavelengths of 470–499 nm [27]. Based on the fact that both iron formulations have this band at approximately the same position, we can conclude that the nature of the iron core is the same and both spectra are compatible with the expected ferric oxyhydroxide mineral form.

The molar extinction coefficients of the absorption bands for each sample were closely similar (Table 1). The peak at 300 nm was best quantitated in undiluted samples analyzed in an optical cell with a path length of 0.001 cm. Calculated extinction coefficients at 300 nm were approximately 2600–3000 M^{-1} cm^{-1} for the two samples. This compares with reported values of 6660 for a different iron–sucrose preparation [19] and 1700 for iron–carrageenan [17]. The shoulder at 470–

500 nm was best quantitated in undiluted sample analyzed in an optical cell with a 0.01 cm path length. The extinction coefficient at 470 nm was approximately 300–400 M^{-1} cm^{-1} for the two samples.

The stability of the iron core structure in each of the iron formulations was assessed by dilution and/or dialysis. Dilution to a concentration of 5 mg Fe/mL, or dialysis against water resulting in a similar dilution, had no significant effect on the spectral shape or molar extinction coefficients of the iron absorption bands (Table 1).

3.2. Transmission electron microscopy (TEM)

TEM micrographs of dialyzed iron–sucrose and dialyzed iron–gluconate samples at equivalent magnifications are compared in Fig. 2. The beadlike iron mineral cores appear to be fairly uniform in size for a given sample. This uniformity reflects the manufacturing processes, and results in particles with a narrow range of sizes. The comparison of the images of two samples shows that the iron–gluconate particles have cores that are generally slightly smaller (Fig. 2(a)) than those of iron–sucrose (Fig. 2(b)).

Measurement of the diameters of the electron dense particles is used to estimate the diameter of the iron mineral core in a given sample. For iron–sucrose, the results indicate a mineral core size distribution ranging from
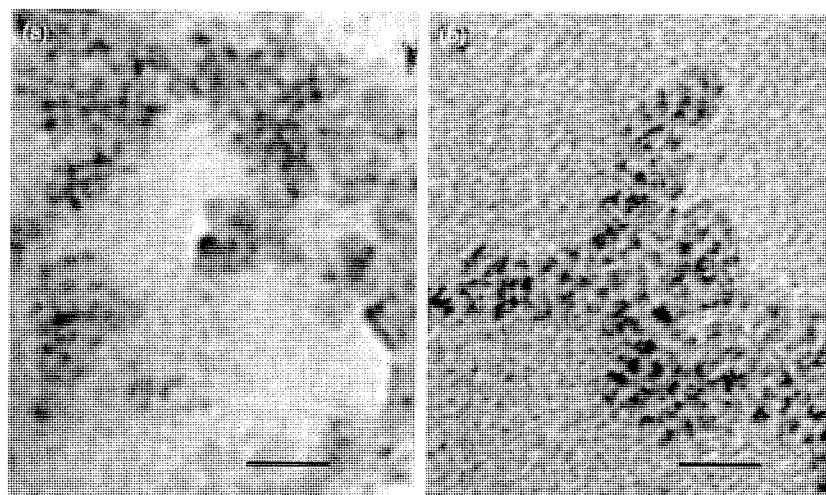

Fig. 2. Transmission electron microscopy image of (a) dialyzed iron–gluconate complex and (b) dialyzed iron–sucrose complex. The bar is 20 nm.
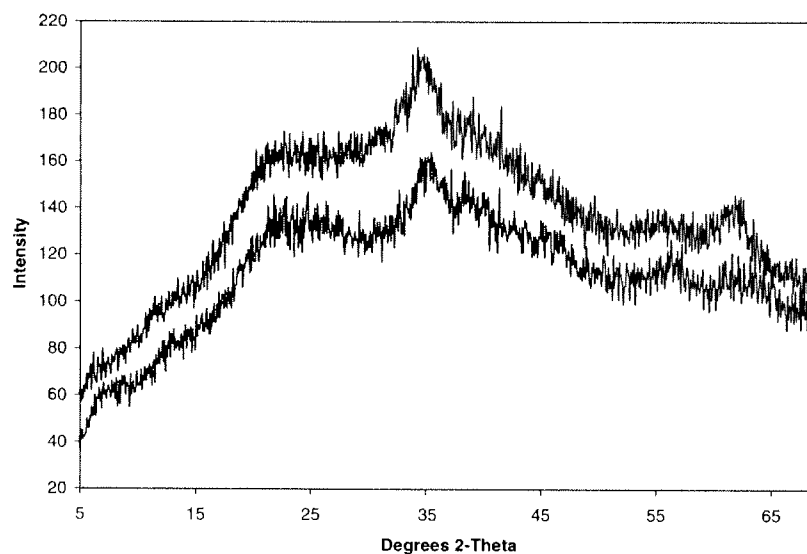
Fig. 3. XRD patterns of iron–sucrose (top) and iron–gluconate (bottom).

of the diffractograms in Fig. 3, it can be also concluded that all peaks broadened evenly, without the presence of a selective peak broadening, i.e., there was no preferential deformation plane due to the complexation with sucrose or gluconate.

It should be mentioned that XRD patterns of both formulations appear to have a very weak diffraction peak from the (002) plane (diffraction angle $2\theta = 61.15°$), which would indicate the presence of Cl^- anions. The presence of Cl^- is in accord with the tunnel-containing akaganeite structure.

On the XRD pattern of iron–sucrose sample after pH-matched dialysis, the sucrose peaks at 11.5° and 22° are almost eliminated (Fig. 4, top spectrum). How-ever, an overall lifting of the area of their presence around 20° confirms that there is still some sucrose in the sample and that the sucrose is not uniformly ordered. Dialysis did not destroy the iron mineral core, since the main reflection attributed to the akaganeite polymorph remains strong after dialysis.

For iron–gluconate, the effect of removing unbound sucrose was more noticeable (Fig. 4, bottom spectrum). In addition to the apparent disappearance of the sucrose peaks at 11.5° and 22°, the pattern of the dialyzed sample has a newly visible akaganeite peak at 26.8°. That difference in the peak appearance between the two dialyzed samples occurs despite the fact that the size of the iron–gluconate core is slightly smaller than that of
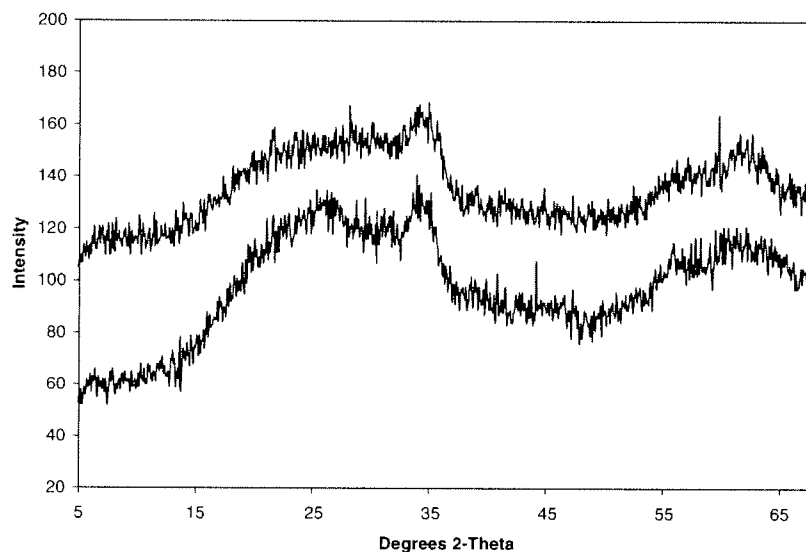

Fig. 4. XRD patterns of dialyzed iron–sucrose (top) and dialyzed iron–gluconate (bottom).
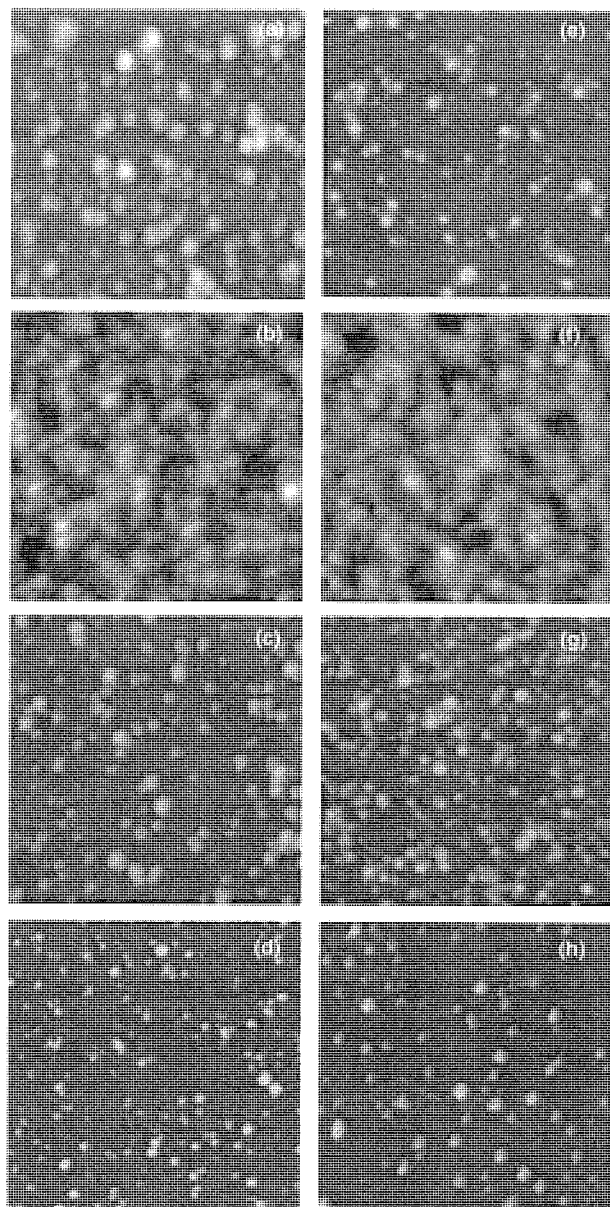
Fig. 6. Atomic force microscope height images of iron–sucrose complex (a–d), and iron–gluconate complex in sucrose (e–h) at various dilutions. Final iron concentrations are 5 mg/mL (top row), 2–2.5 mg/mL (row 2), 0.8–1.3 mg/mL (row 3), and 0.6–0.7 mg/mL (row 4). All image sizes 1 μm × 1 μm, with a color scale covering a height range 8–20 nm in different images.

placement in the vertical direction. In addition, the presence of residual unbound sucrose surrounding each bead on the surface can make the apparent bead diameter larger than the true diameter of the bead.

The effects of dilution and/or dialysis of the iron formulations on the measured particle sizes were investigated. The iron–sucrose sample showed a relatively modest reduction in height with dilution, but a significant decrease in apparent particle width. The initial decrease in average nanoparticle height from 3 to 2 nm,

observed upon dilution to 2 mg Fe/mL, was primarily caused by the fact that the particles were deeply embedded in a sucrose residue covering the surface for that particular sample (Fig. 6(b)). Thus, the measured height in that case is really only the height of the upper part of the particles above the sucrose. That phenomenon can also explain the observation that upon the next dilution to 0.8 mg/mL the average measured height increased again to 3 nm (Fig. 6(c)), in contrast with the logical expectation that upon dilution the particle size would decrease. Upon the final dilution to 0.66 mg/mL the average measured height stayed nearly constant at 3 nm. We conclude that the height of the particles is relatively stable with dilution. The fact that the average height of a whole iron–sucrose particle approximately coincides with the average diameter of the iron mineral core from TEM images indicates the severity of the carbohydrate shell compression and/or displacement by the AFM tip. The corrected iron–sucrose particle diameter, in contrast, decreased significantly from 22 nm at the highest concentration to approximately 6 nm at the lowest concentration. This latter measurement is least affected by unbound but loosely associated sucrose surrounding the beads on the surface. These results were reproduced in a second series of experiments (Table 3) comparing particle size at concentrations of 0.8 and 0.4 mg/mL. The iron–sucrose particles showed no difference in the particle height, but a significant decrease in diameter from 15 to 4 nm. The above observations might mean that dilution below about 0.8 mg/mL, which is a 25-fold dilution of original sample, results in a loosening of weakly bound sucrose. The average final particle size observed at the greatest dilution is therefore approximately 3 nm in height and 4–6 nm in diameter. A similar particle size is obtained for samples dialyzed against water at pH 10 to remove unbound or weakly bound carbohydrates. The dialyzed iron–sucrose particles showed an average height of 3 nm, and apparent width of 7 nm (Fig. 7(a) and Table 3), in good agreement with the dimensions of the particles analyzed at the greatest dilution.

The iron–gluconate particles in sucrose are affected by the same height and width measurement uncertainties as seen for iron–sucrose (Table 4). Dilution from 5 to 2.5 mg/mL results in an apparently significant reduction in height and increase in width. This is partially an artifactual change, resulting from a variable background elevation due to unbound or loosely bound sucrose and gluconate. Disregarding that data point, the particle height decreases only slightly, over the entire range of dilution from 5 to 0.62 mg/mL. The particle apparent width decreased from 12 to 11 nm.

Dialysis of the iron–gluconate formulation against water at pH 8 was effective in further removal of unbound or loosely bound carbohydrate. In three separate experiments, dialysis of iron–gluconate nanoparticles re-

DOCKET ALARM

Explore Litigation Insights

Docket Alarm provides insights to develop a more informed litigation strategy and the peace of mind of knowing you're on top of things.

Real-Time Litigation Alerts

Keep your litigation team up-to-date with **real-time alerts** and advanced team management tools built for the enterprise, all while greatly reducing PACER spend.

Our comprehensive service means we can handle Federal, State, and Administrative courts across the country.

Advanced Docket Research

With over 230 million records, Docket Alarm's cloud-native docket research platform finds what other services can't. Coverage includes Federal, State, plus PTAB, TTAB, ITC and NLRB decisions, all in one place.

Identify arguments that have been successful in the past with full text, pinpoint searching. Link to case law cited within any court document via Fastcase.

Analytics At Your Fingertips

Learn what happened the last time a particular judge, opposing counsel or company faced cases similar to yours.

Advanced out-of-the-box PTAB and TTAB analytics are always at your fingertips.

API

Docket Alarm offers a powerful API (application programming interface) to developers that want to integrate case filings into their apps.

LAW FIRMS
Build custom dashboards for your attorneys and clients with live data direct from the court.

Automate many repetitive legal tasks like conflict checks, document management, and marketing.

FINANCIAL INSTITUTIONS
Litigation and bankruptcy checks for companies and debtors.

E-DISCOVERY AND LEGAL VENDORS
Sync your system to PACER to automate legal marketing.